ELSEVIER

Materials Science and Engineering A 398 (2005) 349–359

MATERIALS SCIENCE & ENGINEERING A

www.elsevier.com/locate/msea

Low-cycle fatigue-induced martensitic transformation in SAF 2205 duplex stainless steel

P.K. Chiu [a], K.L. Weng [b], S.H. Wang [a,*], J.R. Yang [b], Y.S. Huang [a], Jason Fang [c]

[a] *Department of Mechanical Engineering, National Taiwan Ocean University, Keelung 20224, Taiwan*
[b] *Institute of Materials Science and Engineering, National Taiwan University, Taipei, Taiwan*
[c] *Outo Kumpu Asia Pacific, Taipei, Taiwan*

Received 16 November 2004; received in revised form 17 March 2005; accepted 29 March 2005

Abstract

The low-cycle fatigue (LCF) behavior of SAF 2205 duplex stainless steel at the strain amplitudes of 0.9% and 1.5%, combined with strain ratios $R = -1.0$ and -0.2, exhibits a mixed mode of cyclic hardening and cyclic softening as the cycle life increases until failure. The microstructure of the as-received metal is composed of ferrite (α) and austenite (γ) phases with $51\alpha/49\gamma$, vol.%. The evolution of the α/γ phase in the samples treated by all LCF tests has been revealed under the high-resolution transmission electron microscope. Dislocation cell structures and persistent slip bands (PSB) can be observed in the α phase in the samples of all LCF tests. The tangled dislocations accumulated at the stacking faults in the γ phase can be seen in the sample of strain amplitude of 0.9% with $R = -1$. At the same strain amplitude of 0.9% but with $R = -0.2$, the microstructure of the γ phase transforms to the distinct ε-martensite intersected mutually, which is promoted by a higher 0.6% tensile mean strain than the previous strain ratio, $R = -1$, having 0% mean strain. Further, at a relatively higher strain amplitude of 1.5% with $R = -1$, γ-austenite has transformed to the strain-induced thin lath-like α'-martensite sheaths. At the same strain amplitude with $R = -0.2$, the thin lath-like α'-martensite sheaths grows into thicker and longer strain-induced martensite bundles as the tensile mean strain increases from 0% to 1.0%. The strain-induced martensite present at the failure region correlates on intimate terms with the maximum microhardness distribution at the γ-austenite grains of the failure region at strain amplitude of 1.5% with $R = -0.2$. It suggests that the localized transformation of retained austenite into martensite at a tip of a fatigue crack improves the fatigue resistance by either hindering the crack propagation or reducing the crack growth rate.

Keywords: Low-cycle fatigue (LCF); Duplex stainless steel; Strain amplitude; Strain-induced martensite

1. Introduction

The superior properties of duplex stainless steel (DSS), such as high strength, good weldability, and relatively good resistance to stress corrosion and pitting [1,2], come primarily from the almost equal amounts of austenite (γ) and ferrite (α). The fatigue properties of duplex stainless steel have been studied by several researchers [3–5] in recent years. Hayden and Floreen [6] examined the low-cycle fatigue (LCF) hardening and softening response of an ultra fine-grained ferrite–austenite alloy (IN-744). They found that the material exhibited an appreciable hardening during the first few cycles, followed by softening with continued cycling. The LCF properties of the duplex stainless steel at high strain amplitudes approach the basic fatigue mechanisms of the ferrite phase with screw dislocation and pencil glide and approach the cyclic deformation mechanisms of the austenite phase with planar dislocations and planar slip at low strain amplitudes. The phenomena of hardening and softening in duplex stainless steel has been reported by Magnin et al. [7]. Initial hardening is usually attributed to dislocation multiplication and interactions. The cyclic softening subsequent to hardening is attributed to an increase in density of mobile dislocation [8]. The dislocation tangles, pile-ups and planar arrays were the sub-structural features associated with the hardening stage, whereas irregular walls and poorly developed dislocation cell

* Corresponding author. Tel.: +886 2 24622192x3221; fax: +886 2 24620836.
E-mail address: shwang@mail.ntou.edu.tw (S.H. Wang).

0921-5093/$ – see front matter
doi:10.1016/j.msea.2005.03.096

structure were correlated with the softening stage. At low strain amplitudes, the plastic strain is small. Therefore, only a small amount of plastic strain accumulates in each cycle.

Fatigue characteristics of duplex stainless steel at high-cycle fatigue are assumed to be associated with the intense slip bands in the ferrite matrix. Because the applied stress exceeds the fatigue limit, localization of strain accumulates in ferrite. The crack nucleation sites are difficult to discern among the ferrite, austenite grain boundary or α/γ interfaces [9]. During low-cycle fatigue, some cracks are formed at α/γ interfaces, although most of them are located at the ferrite boundaries [10].

Fatigue response of the material is strongly dependent on both the microstructure and the test environment [11]. Microstructure affects the slip and/or twinning modes and the subsequent crack initiation and propagation behavior. Cyclic plastic deformation may alter the microstructure, lead to phase transformation, and influence fatigue performance. Some groups consider that the austenite can transform into brittle martensite under certain cycle stress, thus accelerating crack propagation and decreasing fatigue resistance [1]. Others claim that martensite transformation induced by the strain can increase fatigue resistance [2–5] due to the need to absorb strain energy.

It is well known that the elements carbon and nitrogen play essential roles in the plastic behavior and stabilization of austenite; on the other hand, nitrogen promotes the formation of stacking faults and then of hexagonal ε-martensite phase during straining. Depending on the stacking fault energy, the formation of α′-martensite occurs directly from austenite [12,13] or via the hexagonal ε-martensite phase [14,15].

The aim of this work is to investigate the effects of microstructural evolution of the α and γ phases in duplex stainless steel caused by cyclic plastic deformation on the hardening phenomena embedded in cyclic softening. The effects of strain amplitudes and strain ratios of low-cycle fatigue at 0.25 Hz on martensitic transformation will be investigated and discussed. The purpose of this paper is to focus on investigation of the strain level for induced martensite formation and the types of induced martensite, both associated with the strain amplitude and the mean strain.

2. Experimental procedure

The chemical composition of the SAF 2205, analyzed by Glow Discharge Spectrometer (GDS), is listed in Table 1. The low-cycle fatigue tests, introducing cyclic plastic deformation of experimental duplex stainless steel, were conducted in air using a total strain range ($\Delta\varepsilon$) of 1.8% and 3.0% (corresponding to strain amplitude, $\Delta\varepsilon/2$, at 0.9% and 1.5%, respectively) controlled with two strain ratios at $R = -1$ and -0.2 (listed in Table 2). The loading frequency was fixed at 0.25 Hz. The dimension of the fatigue specimen is schematically presented in Fig. 1, with reference to ASTM E606.

Fractographs of fatigue failure were observed using a HITACHI S-4100 scanning electron microscope (SEM) and operated at 15 kV. Optical metallography was electrolytically etched in 5N NaOH solution at 9 V etching potential for 30 s. The sampling position of thin foils for transmission

Table 1
Chemical composition of the SAF 2205 duplex stainless steel studied (wt.%)

Element	SAF 2205
Cr	21.8
Ni	5.7
Mo	2.9
C	0.02
Si	0.4
Mn	1.43
N	0.150
P	0.023
S	0.002
Cu	0.15

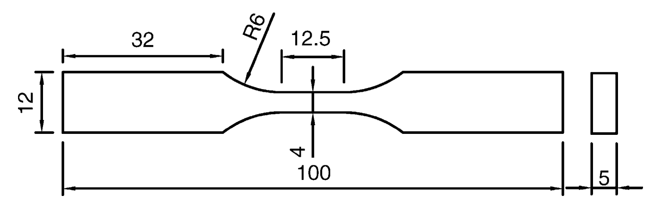

Fig. 1. The dimensions of a fatigue specimen (mm).

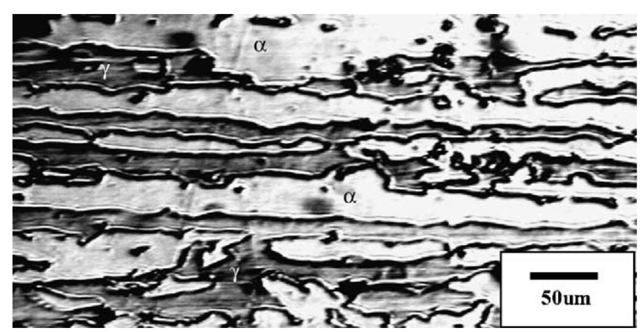

Fig. 2. The optical microstructure of DSS 2205 specimen.

Table 2
The fatigue test parameters in the permanent work

Strain ratio, R	ε_{min} (%)/ε_{max} (%)	Mean strain, ε_{mean} (%)	$\Delta\varepsilon$ (%)	$\varepsilon_a = \Delta\varepsilon/2$ (%)	Life (no. of cycles)
−1	−0.9/0.9	0	1.8	0.9	988
	−1.5/1.5	0	3	1.5	289
−0.2	−0.3/1.5	0.6	1.8	0.9	994
	−0.5/2.5	1.0	3	1.5	239

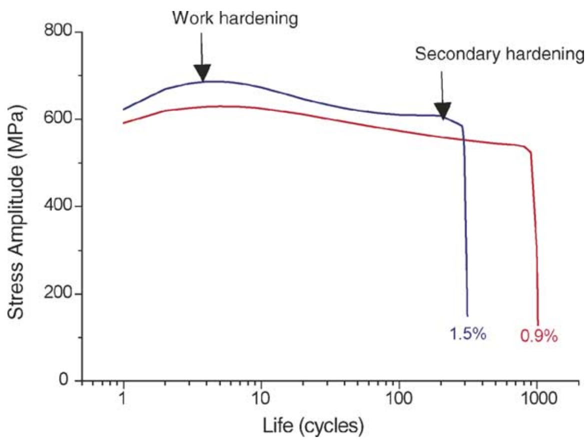

Fig. 3. The peak tensile stress amplitude versus number of cycles at different strain amplitudes with strain ratio, $R = -1$.

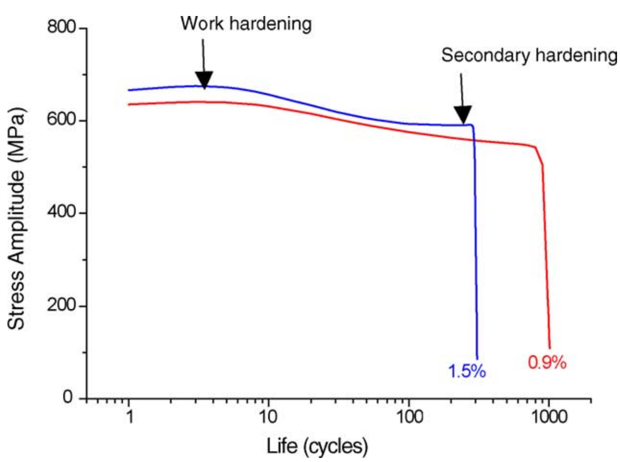

Fig. 4. The peak tensile stress amplitude versus number of cycles at different strain amplitudes with strain ratio, $R = -0.2$.

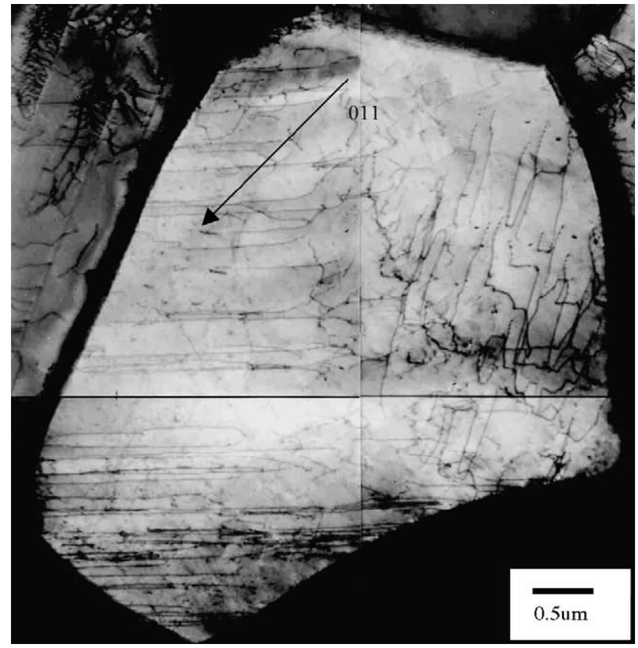

Fig. 5. Dislocation structure in α-ferrite of as received 2205 DSS. Observation under two-beam condition, $\vec{g} = [0\,1\,1]$.

electron microscopy (TEM) examination was taken from the fatigue failure region. A sliced specimen was ground down to 0.06 mm by abrasion on SiC papers and then punched to a disk. A 3-mm punched disk was electro-polished to a thin foil in a solution composed of 5% perchloric acid, 25% glycerol, and 70% ethanol using a twin-jet at the environmental temperature within −5 to −10 °C and the etching potential at 45 voltage. The high-resolution microstructures and microanalyses of the fatigued specimens were investigated using a JOEL JEM 2000 EX II equipped with an energy-dispersive

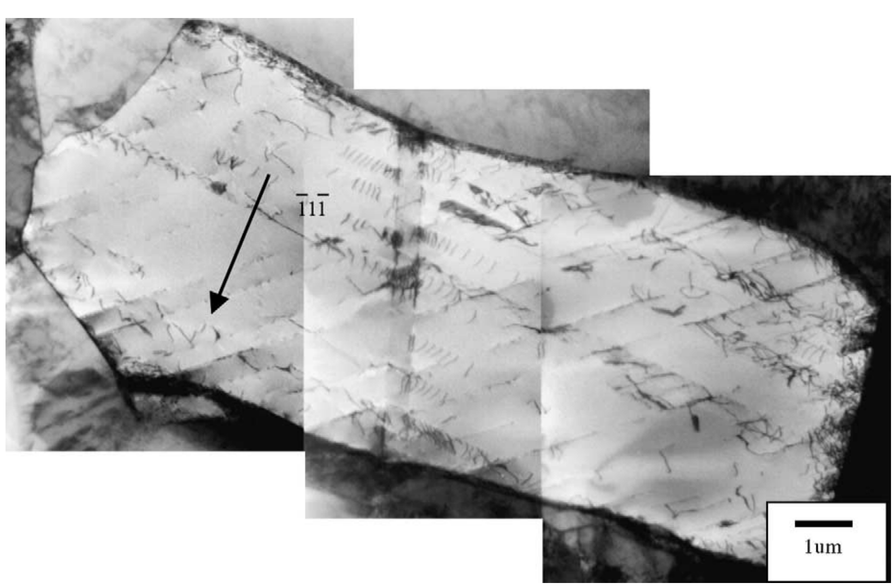

Fig. 6. Dislocation structure in γ-austenite of as-received 2205 DSS. Observation under two-beam condition, $\vec{g} = [\bar{1}\,1\,\bar{1}]$.

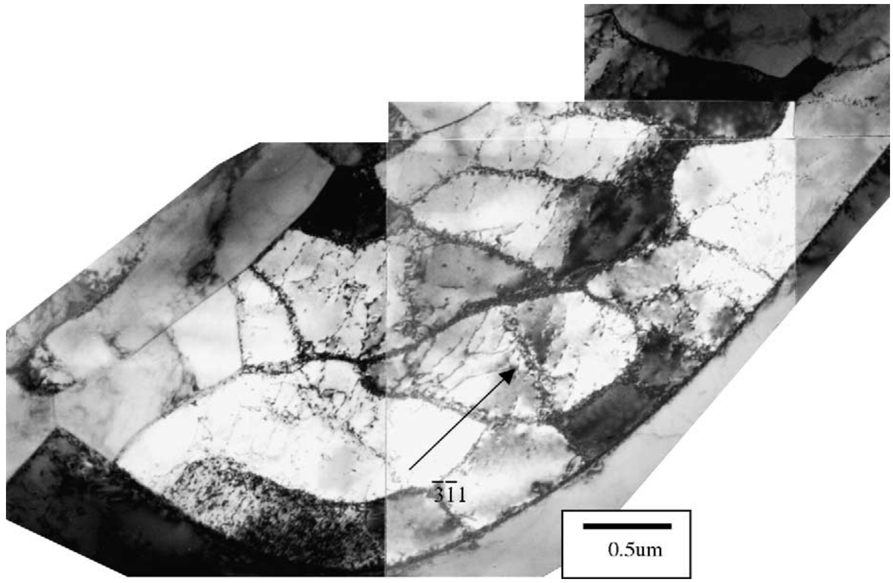

Fig. 7. Dislocation sub-structure in α-ferrite of the specimen fatigued at $R = -1$, $\varepsilon_a = 0.9\%$. Observation under two-beam condition, $\vec{g} = [\bar{3}\,\bar{1}\,1]$.

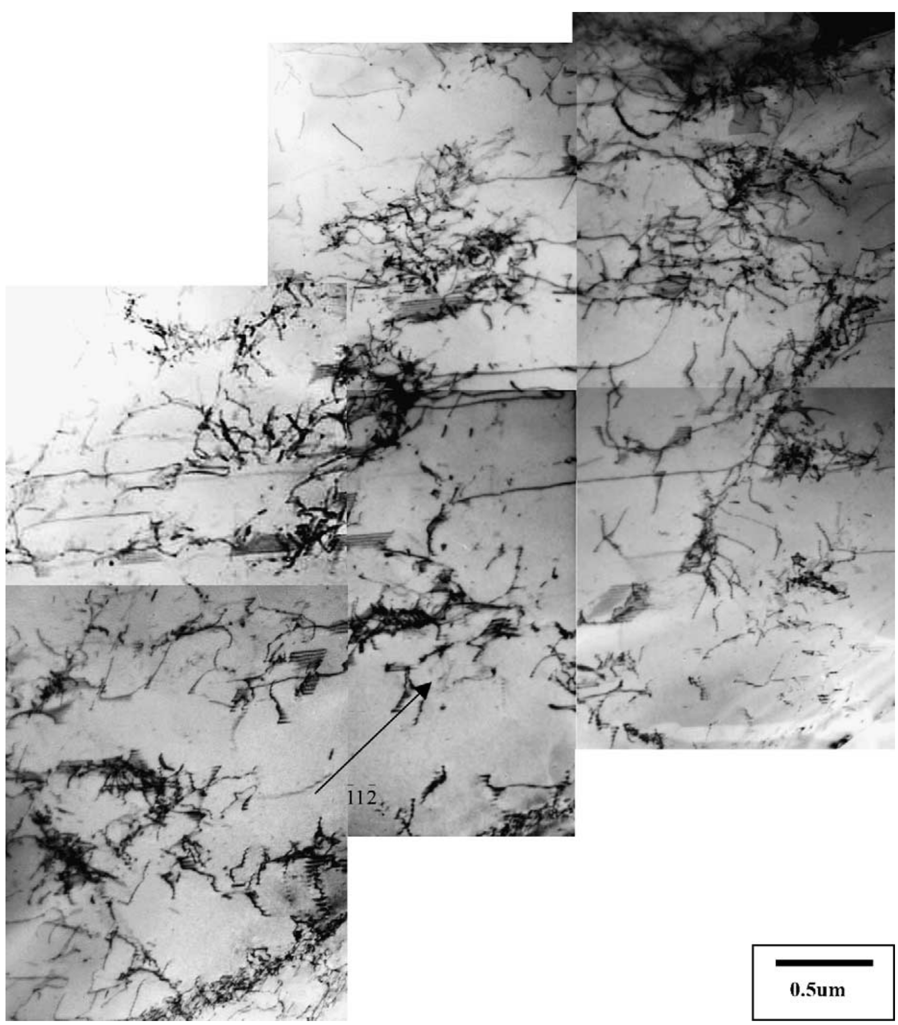

Fig. 8. Dislocation structure in γ-austenite of the specimen fatigued at $R = -1$, $\varepsilon_a = 0.9\%$. Observation under two-beam condition, $\vec{g} = [\bar{1}\,1\,\bar{2}]$.

X-ray spectrometer (EDS). The Vickers microhardness was measured at the middle of the fatigued specimens from the fractured end toward the grip end across the α and γ phases (Fig. 2) under a constant load of 300 g.

3. Results and discussion

The variation in peak tensile stress amplitude with the number of cycles during the fatigue process at strain amplitudes of 0.9% and 1.5% with strain ratio, $R = -1$ is shown in Fig. 3, and that with strain ratio, $R = -0.2$ is shown in Fig. 4. They reveal a mixed softening and hardening mode (Figs. 3 and 4) at different strain amplitudes and strain ratios. In other words, the peak stress evolves an increase, cyclic hardening, at several beginning cycles of the test, followed by a decreasing peak stress, cyclic softening with continued cycling. To achieve cyclic softening requires a high density of mobile dislocations [8,16] by demanding a higher plastic strain. The higher the cyclic strain range, the larger the plastic strain component is, and this leads to a high density of mobile dislocations. A secondary hardening appears at strain amplitude of 1.5% only for both strain ratios (shown in Figs. 3 and 4). In contrast, the cyclic softening phenomenon disappears until fracture at strain amplitude of 0.9% for both strain ratios $R = -1$ and -0.2. The early distinct cyclic hardening, especially, at 1.5% strain amplitude, is attributed to dislocation multiplication and their mutual interactions. The secondary hardening at 1.5% amplitude shown in Figs. 3 and 4 is associated with the formation of strain-induced martensite [17–20], which will be discussed later.

LCF behavior of a duplex alloy can be attributed to the deformation mechanisms and the fatigue properties of the austenitic and ferritic phases. The evolution of high-resolution microstructures of cyclic plastic deformation was observed at the α and γ phases at strain amplitudes of 0.9% and 1.5% combined with $R = -1$ and -0.2, respectively. As-received DSS reveals few planar dislocation arrays and pile-ups in both BCC α grains (Fig. 5) and FCC γ grains (Fig. 6) under two-beam condition. The initial well-defined cell structure of dislocations due to cross slipping in screw dislocation is developed in α grains at strain amplitude of 0.9% with strain ratio, $R = -1$, as shown in Fig. 7. In contrast, the tangled planar dislocation and some stacking faults appear in the FCC γ grains, at the same fatigue condition of strain amplitude of 0.9% with strain ratio, $R = -1.0$, shown in Fig. 8. The much smaller size of cell sub-structure and persistent slip bands (PSB) emerge in the α-ferrite phase for the specimen fatigued at a strain amplitude of 0.9% with $R = -0.2$ in Fig. 9. Many intersected bands of ε-martensites are formed in γ-austenite phase at strain amplitude of 0.9% with $R = -0.2$, shown in Fig. 10. Although the strain amplitude is the same for Figs. 7–10, a distinct microstructure results from a higher tensile mean strain ($\varepsilon_{\mathrm{mean}}$) of 0.6% at $R = -0.2$ (Figs. 9 and 10) rather than the mean strain of 0% at $R = -1$ (Figs. 7 and 8).

When the cyclic strain amplitude increases to 1.5% with $R = -1$, equivalent to 0% mean strain, the microstructure of α-ferrite phase exhibits smaller cell sub-structures and more persistent slip bands as compared with those in 0.9% strain amplitude. The smallest dislocation cell size and the most dense persistent slip bands exists in the α phase at the strain amplitude of 1.5% with $R = -0.2$ having 1.0% tensile mean strain. In contrast, at the relatively higher strain amplitude of 1.5% with $R = -1$ and -0.2, strain-induced lath-like α′-martensite, i.e. mechanical bring-out martensite, is found in the major γ phases (Figs. 11 and 12). It seems that the strain-induced martensite nucleates and grows from the boundary (Figs. 11 and 12). Comparing Fig. 11 with Fig. 12 reveals that the amount of martensite increases with increasing strain ratios from $R = -1$ to -0.2, and the thickness and length of the lath in martensite sheaths become thicker and longer with $R = -0.2$ than those with $R = -1$. The secondary hardening exhibited at 1.5% strain amplitude at higher cycles before fracture in the plots of peak stress versus life curve (Figs. 3 and 4) for both R ratios should be correlated with this cyclic plastic deformation-induced martensite (Figs. 11 and 12) because of the large accumulated plastic strain and stored energy at higher strain amplitudes. However, there was no martensite found in the γ phase at the lower strain amplitude of 0.9% with two strain ratios, besides tangled dislocations and dislocations accumulated at the stacking faults (Fig. 8). The microstructure without martensite present explains why the peak stress declined until fracture without a secondary hardening at 0.9% strain amplitude for the two strain ratios (Figs. 3 and 4).

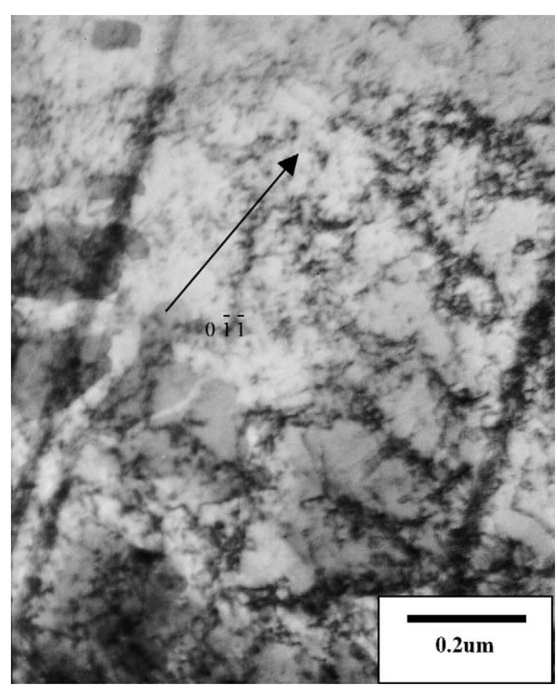

Fig. 9. Dislocation sub-structure in α-ferrite of the specimen fatigued at $R = -0.2$, $\varepsilon_a = 0.9\%$. Observation under two-beam condition, $\vec{g} = [0\bar{1}\bar{1}]$.

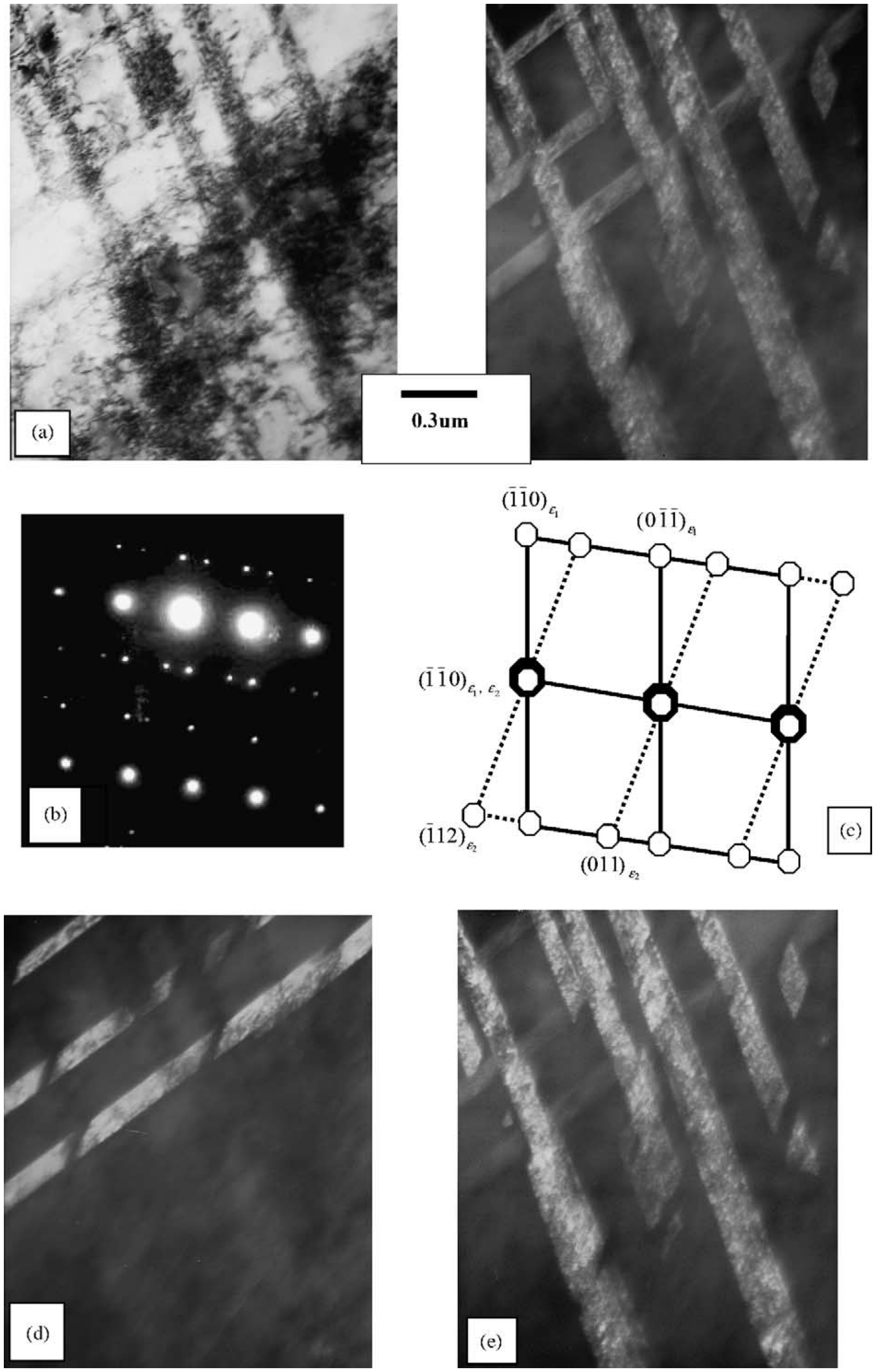

Fig. 10. TEM showing strain-induced ε-martensite from the γ-austenite observed in the fracture zone of the specimen fatigued at $R = -0.2$, $\varepsilon_a = 0.9\%$: (a) BF image; (b) diffraction pattern zone $[\bar{2}\,\bar{1}\,1]$; (c) interpretation of the diffraction pattern (b); (d) DF image of ε_1-martensite; (e) DF image of ε_2-martensite.

As mentioned above, there is more and thicker martensite at a strain ratio of $R = -0.2$ (Fig. 12) than at a strain ratio of $R = -1$ (Fig. 11) at the same strain amplitude of 1.5%. These results correlate with the curve of peak stress versus life in Fig. 4, in which a sharp corner of the secondary hardening appears at $R = -0.2$ with 1.5% strain amplitude. As seen in Table 2, the mean strain ε_{mean} $(\varepsilon_{max} + \varepsilon_{min})/2)$ increases from 0% at $R = -1$ to 1.0% at $R = -0.2$, which corresponds to a large amount of cyclic tensile strain applied at strain ratio, $R = -0.2$. Therefore, the mean strain shifts toward a positive tensile strain direction at $R = -0.2$, indicating that the material bears more strain energy in tension than in compression to assist active dislocation multiplication and cross slip.

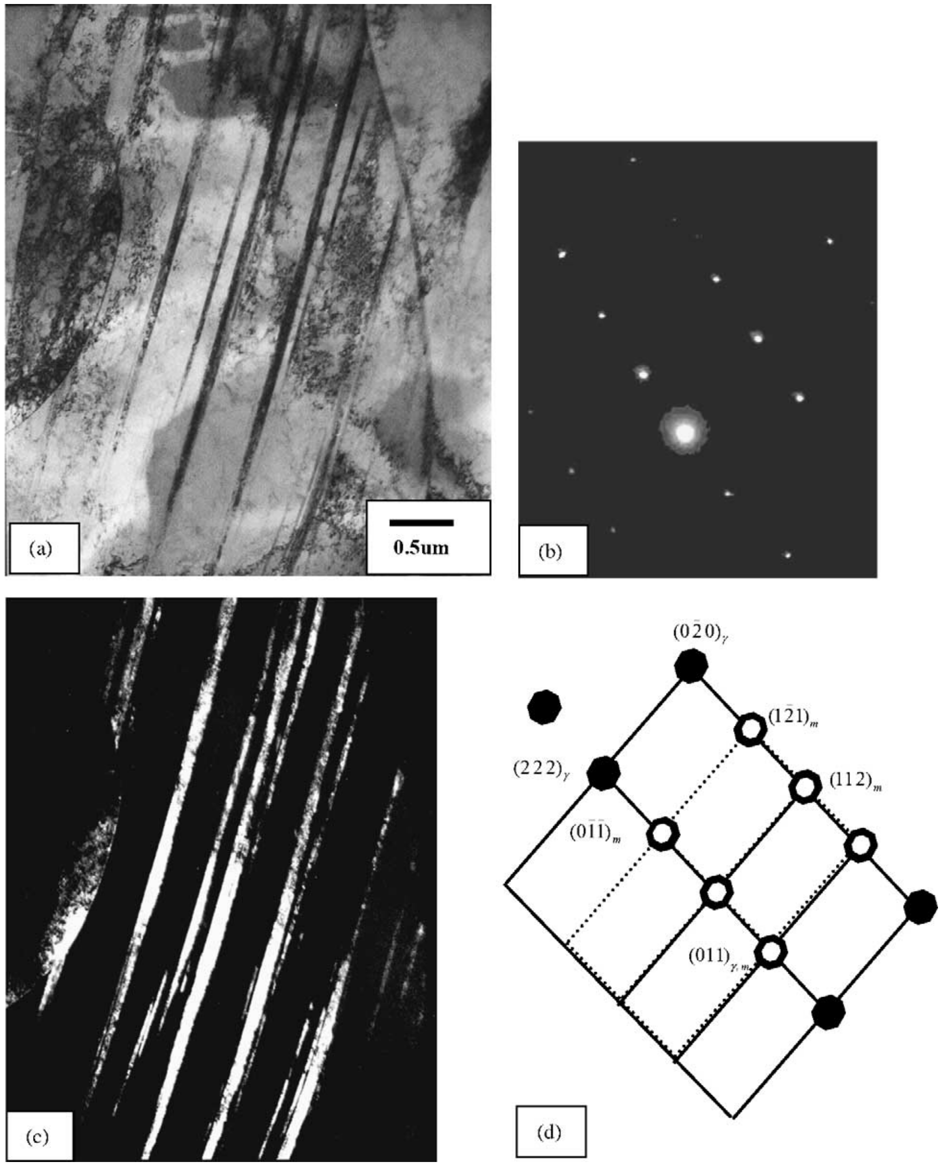

Fig. 11. TEM showing martensite formation from austenite in the specimen fatigued at $R = -1$, $\varepsilon_a = 1.5\%$: (a) BF image; (b) diffraction pattern austenite zone [3 0 1]; martensite zone $[\bar{3}\,\bar{1}\,1]$; (c) DF image; (d) interpretation of the diffraction pattern (b).

Bauadry [21] reported that when the temperature was lower than deformed martensite transformation temperature, $M_d \approx 373$ K and the cyclic plastic strain amplitude ($\Delta\varepsilon_p/2$) was larger than a critical value of ($\Delta\varepsilon_p^c/2$), $\gamma \rightarrow \alpha'$, martensitic transformation occurred under strain-controlled conditions in Fe–18Cr–6.5Ni–0.19C stainless steel [22]. At low-cycle fatigue, a great amount of energy is induced by a relatively high cyclic plastic strain amplitude and more positive tensile mean strain. The high cyclic tensile-deformation facilitates increases in operative microscopic shear band (deformation twins, stacking-fault bundles and ε-martensite) intersection. The intersection is regarded as an effective site for strain-induced martensite nucleation [15]. Therefore, the fact of the foregoing induces martensite nucleation and growth, and prompts the austenite to transform into martensite [15], which is also called mechanical bring-out martensite [6].

Fig. 13a illustrates the microhardness measured across α and γ grains at the middle of fatigue-ruptured specimens from the fracture end. The values of microhardness in the γ and α phases versus distance are plotted in Fig. 13b and c, respectively. As can be seen, the hardness decays exponentially from the rupture end toward the grip end. The maximum value of microhardness distribution happens at 1.5%, the highest strain amplitude with $R = -0.2$, equivalent to a tensile mean strain of 1.0%, for both γ grains (Fig. 13b) and α grains (Fig. 13c). This corresponds to the thicker and longer strain-induced lath martensite bundles existing in the γ grains (shown in Fig. 12) and the smallest dislocation cell size combined with the most dense persistent slip bands in α grains.

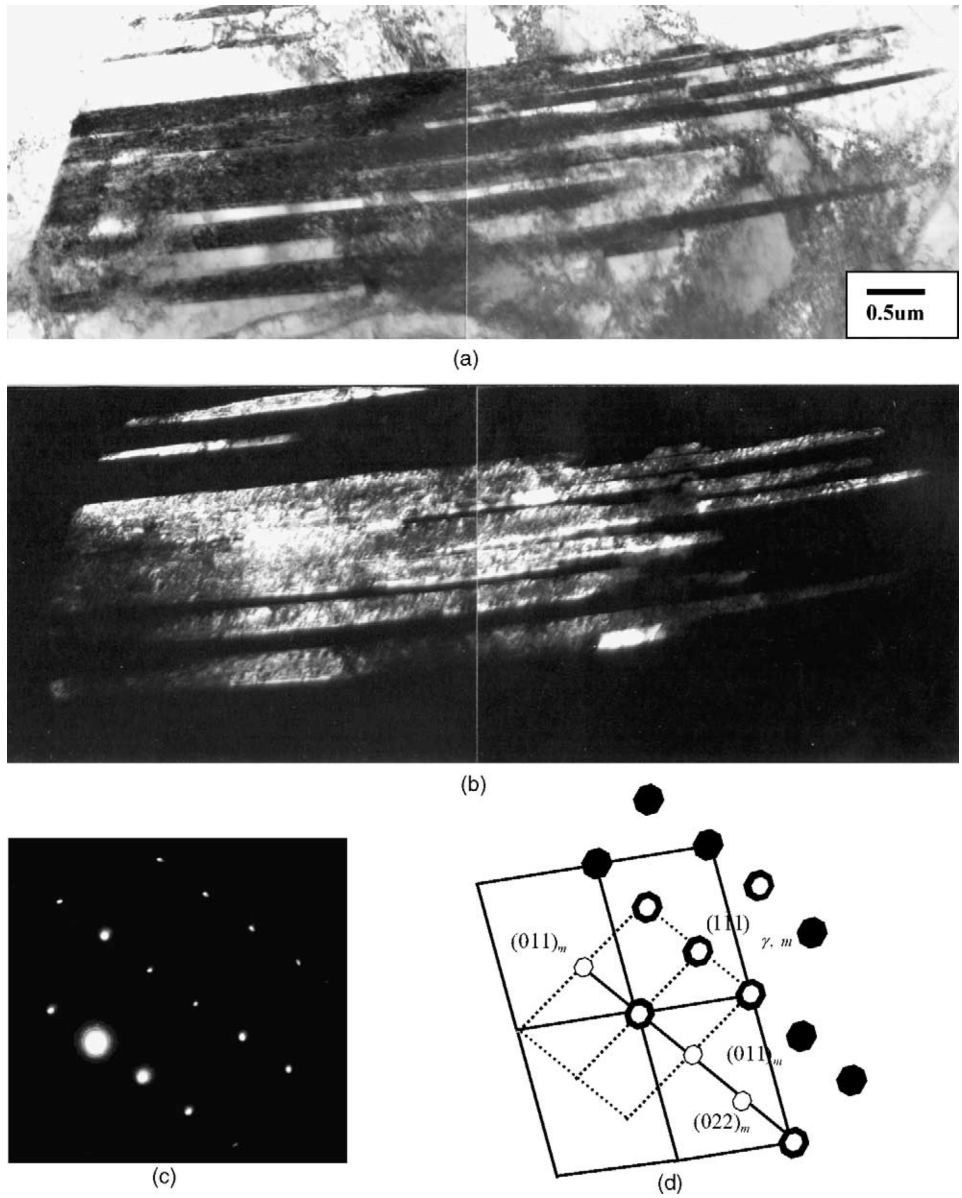

Fig. 12. TEM showing martensite formation from austenite in the specimen fatigued at $R = -0.2$, $\varepsilon_a = 1.5\%$: (a) BF image; (b) DF image; (c) diffraction pattern austenite zone $[\bar{3}\,\bar{2}\,1]$; martensite zone $[\bar{2}\,\bar{1}\,1]$; (d) interpretation of the diffraction pattern.

The next maximum value of microhardness distribution occurs at 1.5%, the highest strain amplitude, but with $R = -1$ having a mean strain of 0% for both γ grains (Fig. 13b) and α grains (Fig. 13c). The results match the thin lath-like strain-induced α′-martensite sheaths in γ grains (shown in Fig. 11) and the smaller dislocation cell size combined with more dense persistent slip bands in α grains. The hardness ranking in third place is the condition of strain amplitude of 0.9% with $R = -0.2$, equivalent to a tensile mean strain of 0.6%, for both γ grains (Fig. 13b) and α grains (Fig. 13c). This corresponds with the intersected ε-martensite formed in γ grains (shown in Fig. 10) and the larger dislocation cell size combined with a few persistent slip bands in α grains (shown in Fig. 9). The lower hardness profile present at a strain amplitude of 0.9% with $R = -1$ is equivalent to a tensile mean strain of 0%, for both γ grains (Fig. 13b) and α grains (Fig. 13c). This trend tallies with the facts that the tangled planar dislocations are mixed with some stacking faults in γ grains (shown in Fig. 8) and that initial well-defined cell structure of dislocations has developed in α grains (shown in Fig. 9). As-received DSS has the minimum value of microhardness in two phases corresponding to few planar dislocation arrays and pile-ups present in both BCC α grains (Fig. 5) and FCC γ grains (Fig. 6). The results of Fig. 13 indicate that the magnitudes of mean strain, strain ratio and strain amplitude play very important roles in low-cycle fatigue. The amount of aforementioned mechanical bring-out martensite (strain-induced martensite) in the γ phase, and the size of dislocation

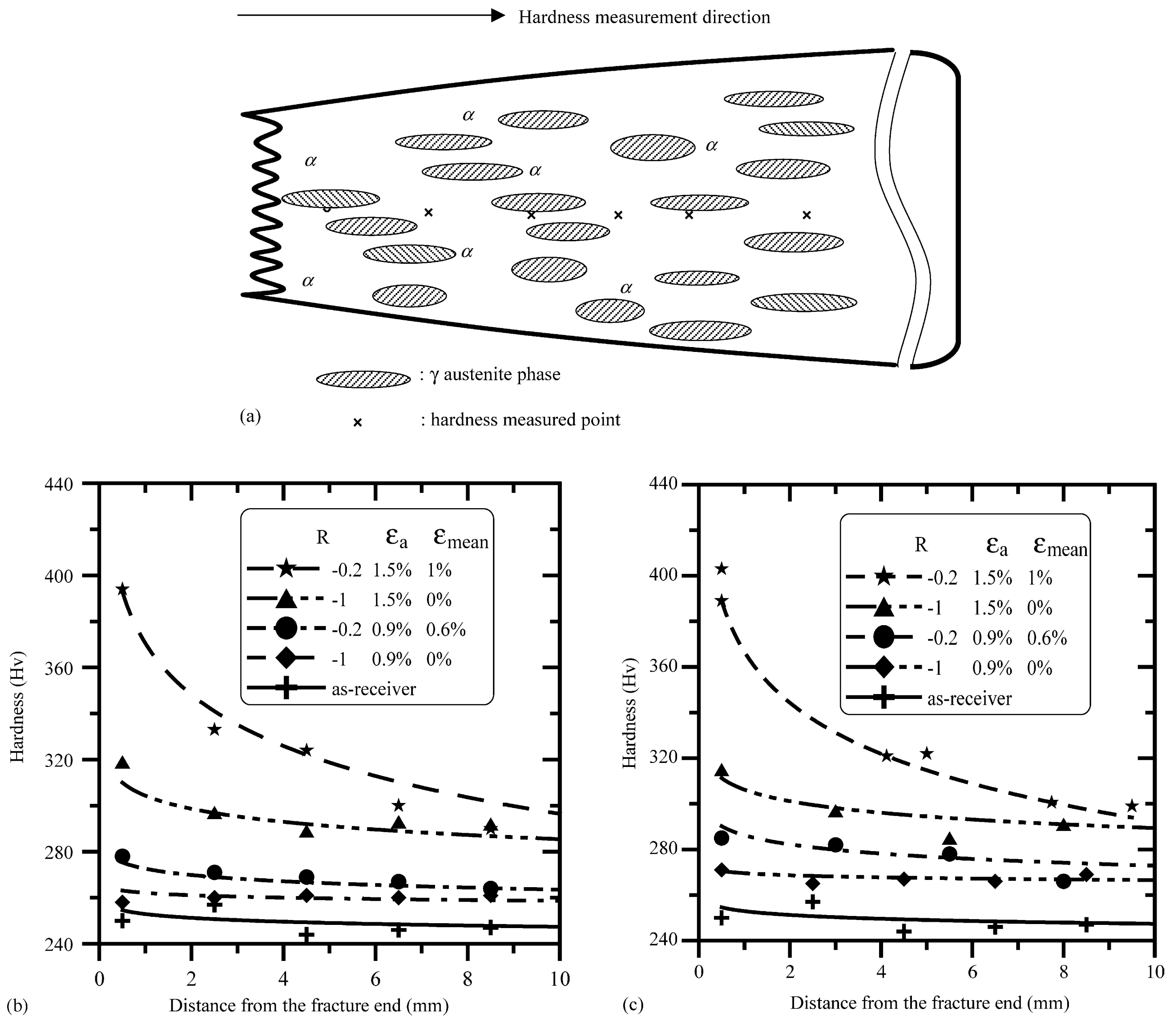

Fig. 13. Summary of microhardness profiles at various fatigue conditions: (a) schematic illustration of microhardness measurement direction and location in (b) γ phase and (c) α phase.

cells coupled with the number of persistent slip bands in the α phase, should affect and contribute to the low-cycle fatigue properties of duplex stainless steel. In short, higher plastic strain amplitude, joined with a higher tensile mean strain would enhance the strain-induced martensite formation resulting in higher hardness. It suggests that the localized transformation of retained austenite into martensite at the tip of a fatigue crack improves the fatigue resistance by either hindering the crack propagation or reducing crack growth rate. Furthermore, the secondary hardening results in a relatively short life in Figs. 3 and 4 at 1.5% high strain amplitude, compared with 0.9% strain amplitude. This is because the martensite boundary is the low energy path for fatigue crack propagation [23].

The fracture surfaces of LCF specimens at different test parameters were examined at the origin zone, middle zone, and overload zone, respectively. The results (Fig. 14) indicate that the origin is more ductile at a low strain amplitude of 0.9% than at a high strain amplitude of 1.5%. Under the same strain amplitude of 0.9%, the fracture feature of the origin with a strain ratio of $R = -1$ having 0% mean strain (Table 2) is characterized by dense debris-like ductile ridges (Fig. 14a), rather than by the coarse ductile ridges (Fig. 14b), with a strain ratio of $R = -0.2$ having a tensile mean strain of 0.6% (Table 2). On the other hand, at a large strain amplitude of 1.5%, the fracture feature with both strain ratios $R = -1$ and -0.2 demonstrates the quasi-cleavage containing some inter-granular cracks (Fig. 14c and d). The fractographs of the middle zone for all specimens reveal a shallow ductile feature. The characteristic of final rupture at 1.5% strain amplitude exhibits a lot of holes, shown in Fig. 14d, with strain ratio, $R = -0.2$ having a tensile mean strain of

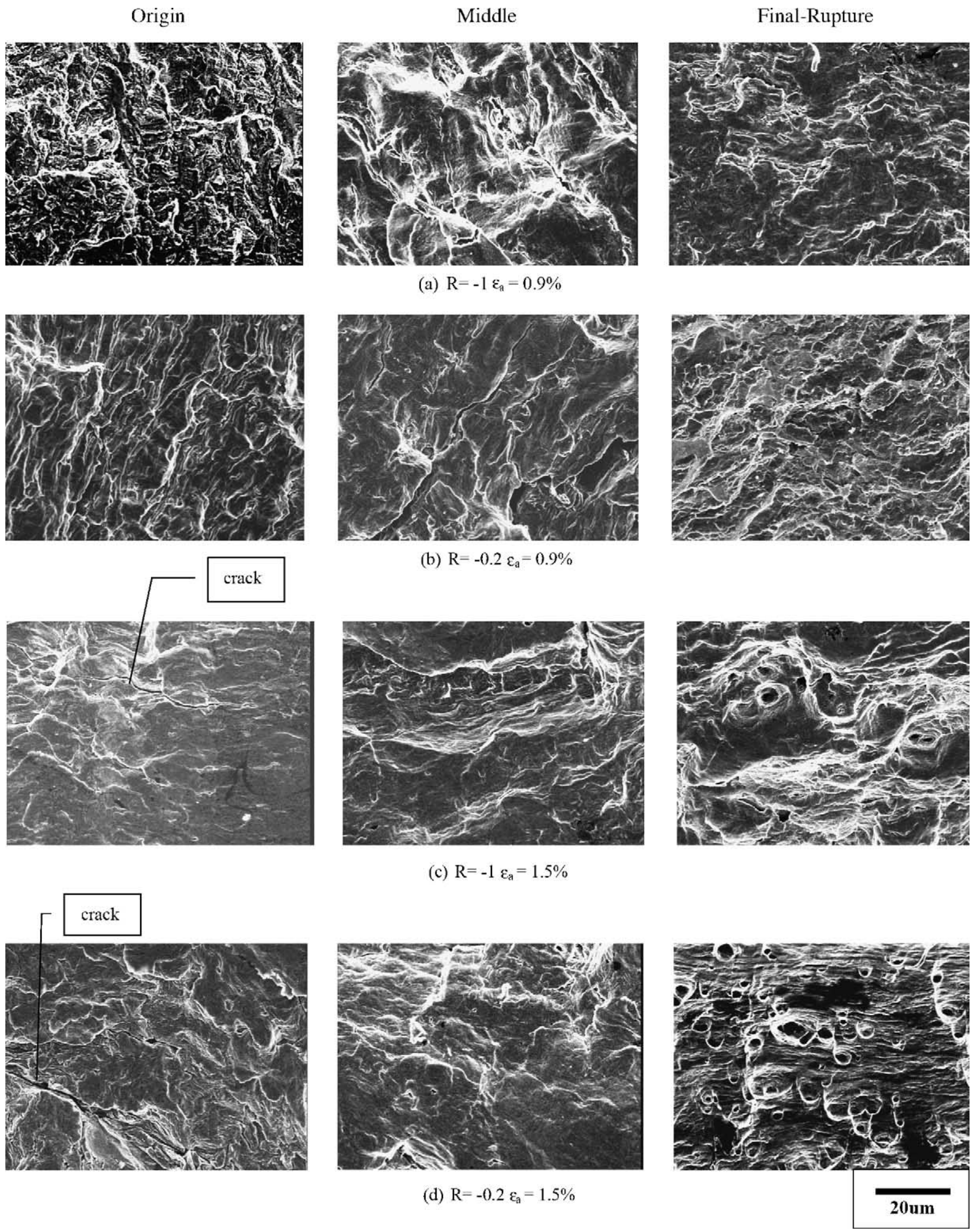

Fig. 14. Fractographs of SAF 2205 as-received metal after fatigue at strain amplitude $\varepsilon_a = 0.9\%$ for: (a) $R = -1$; (b) $R = -0.2$ and strain amplitude $\varepsilon_a = 1.5\%$; (c) $R = -1$; (d) $R = -0.2$.

1.0% (Table 2) rather than with strain ratio, $R = -1$ having zero mean strain (Table 2). It suggests that the number of holes depends on the amount of cyclic plastic deformation-induced martensite. More martensite results in more holes formed after low-cycle fatigue. The lack of holes found for the lower strain amplitude of 0.9% with two strain ratios (Fig. 14) should be due to the absence of induced martensite.

4. Conclusions

(1) The trend of peak stress versus number of cycles for duplex stainless steel shows a mixed mode of low-cycle fatigue. A secondary hardening is found only at the relatively high stain amplitude of 1.5%.
(2) The maximum value of microhardness distribution happens at 1.5%, and the highest strain amplitude with $R = -0.2$, equivalent to a tensile mean strain of 1.0%, for both γ grains and α grains. This corresponds to the thicker and longer strain-induced lath martensite bundles existing in γ grains, and the smallest dislocation cell size combined with the most dense persistent slip bands in α grains.
(3) The next maximum value of microhardness distribution occurs at 1.5%, the highest strain amplitude, but with $R = -1$ having a mean strain of 0%, for both γ grains and α grains. These results match the thin lath-like strain-induced martensite sheaths in γ grains and the smaller dislocation cell size combined with more dense persistent slip bands in α grains.
(4) The hardness ranking in third place is the condition of strain amplitude 0.9% with $R = -0.2$, equivalent to a tensile mean strain of 0.6%, for both γ and α grains. This corresponds to the intersected twinning bands of ε-martensite formed in γ grains and the larger dislocation cell size combined with a few persistent slip bands in α grains.
(5) A higher tensile mean strain would enhance the strain-induced martensite formation, resulting in higher hardness. The feature of all fatigued fractures reveals the ductile mode. In the overload zone, the number of holes depends on the amount of cyclic plastic deformation-induced martensite.
(6) As shown in Table 2, the optimal performance of fatigue life given the longest life, 994 cycles, happened at 0.6% tensile mean strain with strain amplitude 0.9% under strain ratio, $R = -0.2$. It results from the presence of many fatigue-induced intersected ε-martensite bands, which is more beneficial and preferential than the α′-martensite.

Acknowledgements

This work was carried out with financial support from the National Science Council of Taiwan, ROC, through Contracts NSC-91-2216-E-019-009, NSC-92-2216-E-019-010 and NSC-93-2216-E-019-003.

References

[1] S. Mocarski, Metal Prog. 98 (30) (1970) 96–98.
[2] M.K. Kang, Bainite in Steel, Shanghai Science and Technology Press, Shanghai, 1960, pp. 339–380.
[3] D.E. Diesburg, SAE Trans., 780771 (87) (1979) 2907–2916.
[4] H.L. Gao, Y.X. Tan, X.T. Wang, Acta Metall. 24 (1) (1988) A17–A23.
[5] J.X. Dong, R.F. Fang, L.X. Hang, Heat Treat. Metals (9) (1983) 32–36.
[6] H.W. Hayden, S. Floreen, Metall. Trans. 4 (1973) 561.
[7] T. Magnin, J.M. Lardon, L. Condreuse, in: H.D. Solomon, G.R. Halford (Eds.), Low Cycle Fatigue, vol. 942, ASTM STP, ASTM, Philadelphia, PA, 1988, p. 812.
[8] N.J. Ho, Mater. Sci. Eng. 94 (1987) 195–202.
[9] L. Llanes, A. Mateo, P. Violan, J. Méndez, M. Anglada, Mater. Sci. Eng. A234–236 (1997) 850–852.
[10] G.S. Reis, A.M. Jorge Jr., O. Balancin, Mater. Res. 3 (2) (2000) 31–35.
[11] S.G.S. Raman, Int. J. Fatigue 17 (4) (1995) 271–277.
[12] K. Tsuzaki, T. Maki, I. Tamura, Phys. Colloque C4 43 (Suppl. 12) (1982) 423–428.
[13] J. Singh, J. Mater. Sci. 20 (1985) 3157–3166.
[14] P.L. Mangonon, G. Thomas, Metall. Trans. 1 (1970) 229–242.
[15] L.E. Murr, K.P. Staudhammer, S.S. Hecker, Metall. Trans. A 13 (1982) 627–635.
[16] N.J. Ho, S.C. Tjong, Mater. Sci. Eng. 94 (1987) 195.
[17] P. Marmy, T. Leguey, I. Belianov, M. Victoria, J. Nucl. Mater. 283 (2000) 602–606.
[18] W.S. Lee, C.F. Lin, Mater. Sci. Eng. A241 (1998) 48–59.
[19] H.X. Shang, H.J. Ding, Eng. Fract. Mech. 54 (1) (1996) 1–9.
[20] M. Botshekan, S. Degallaix, Y. Desplanques, J. Polak, Fatigue Fract. Eng. Mater. Struct. 21 (1998) 651–660.
[21] R.W. Landgraf, Fatigue and Microstructure, American Society for Metals, OH, 1979, pp. 439–466.
[22] G. Baudry, A. Pineau, Mater. Sci. Eng. 28 (1977) 229–242.
[23] Z.Z. Hu, M.L. Ma, T.Q. Liu, J.H. Liu, Int. J. Fatigue 19 (8-9) (1997) 641–646.